Chinese Chemical Letters 34 (2023) 108159

Contents lists available at ScienceDirect

Chinese Chemical Letters

journal homepage: www.elsevier.com/locate/cclet

New insight into the synergy of nitrogen-related sites on biochar surface for sulfamethoxazole adsorption from water

Chuanbin Wang[a], Lingchao Kong[b], Yanshan Wang[a], Xiaoqiang Cui[a], Ning Li[a,c,*], Beibei Yan[a], Guanyi Chen[a,d,e]

[a] School of Environmental Science and Engineering/Tianjin Engineering Research Center of Bio Gas/Oil Technology, Tianjin University, Tianjin 300072, China
[b] School of Environmental Science & Engineering, Southern University of Science and Technology, Shenzhen 518055, China
[c] Georgia Tech Shenzhen Institute, Tianjin University, Shenzhen 518071, China
[d] School of Mechanical Engineering, Tianjin University of Commerce, Tianjin 300134, China
[e] School of Science, Tibet University, Lhasa 850012, China

ARTICLE INFO

Article history:
Received 19 October 2022
Revised 1 January 2023
Accepted 25 January 2023
Available online 28 January 2023

Keywords:
Synergy
Pyrrolic N
Pyridinic N
Biochar
Adsorption

ABSTRACT

In-depth exploration of the relationship among different adsorption sites is conducive to design of efficient adsorbents for target pollutants removal from water. In this study, the experiments, multivariate non-linear regression and density functional theory calculations are applied to explore the possible synergistic effects of three nitrogen (N)-containing sites on cow dung biochar surface for sulfamethoxazole (SMX) adsorption. Notably, a strong synergistic effect between pyridinic N and pyrrolic N sites was found for sulfamethoxazole adsorption. The adsorption energies of SMX on four pyrrolic N-coupled pyridinic N structures were −1.02, −0.41, −0.49 and −0.72 eV, much higher than the sum of adsorption energies (−0.31 eV) on pyrrolic N and pyridinic N. Besides, the alteration of Mulliken charge revealed that the simultaneous presence of pyridinic N and pyrrolic N improved the electron transfer remarkably from −0.459 e and 0.094 e to −0.649 e and 0.186 e, benefiting for SMX adsorption. This work firstly explored the possible synergies of adsorption sites on biochar surface for organic contaminants removal from water, which shed new lights on the adsorption mechanism and provided valuable information to design efficient adsorbents in the field of water treatment.

Recently, considerable attention has been paid to the water pollution owing to the rapid population growth and advances in industrial [1–3]. Sulfamethoxazole (SMX) is one of the most commonly detected antibiotics in wastewater [4]. Besides, exposing to SMX could result in the emerge of resistant genes and bacteria, posing serious threats to human health [5]. The adsorption process is widely applied for organic pollutants removal due to simple design, convenient operation and high efficiency [6–10]. Besides, it is urgent to develop highly efficient adsorbents with high adsorption capacity and fast adsorption kinetics [11]. Biochar usually exhibits huge specific surface area (SSA) and abundant functional groups, which is conducive to the adsorption of organic contaminants. The biochar is mainly made from waste biomass, regarding as a cost-effective and environmental-friendly adsorbent [12].

The adsorption sites on biochar surface consist of oxygen-, nitrogen (N)-, carbon-related sites and defects. As far as we know, the dominant adsorption sites, and interactions between active sites and pollutants have been investigated broadly [13]. Most studies have only focused on a single adsorption site when exploring the contact pattern with pollutants. For example, pyridinic N was involved in hydrophobic effect, while pyrrolic N could combine with organics through hydrogen bond [14]. In addition, graphite N adsorbs organic pollutants mainly through π-π electron donor-acceptor interactions [15].

However, no study has concentrated on the possible interactions among different adsorption sites. The synergy among different adsorption sites, especially those containing the same element, might exist in the process of adsorption due to electron transfer. Therefore, to explore the relationship among different adsorption sites would benefit for directional regulation of active sites on biochar surface, realizing efficient adsorption of target pollutants.

Herein, we select N-related adsorption sites on cow dung derived biochar surface as an example to investigate the possible interactions. The relationships among pyridinic N, pyrrolic N and graphitic N sites are determined by constructing a multivariate nonlinear mathematical model. Furthermore, the adsorption

* Corresponding author.
E-mail address: liningec@tju.edu.cn (N. Li).

https://doi.org/10.1016/j.cclet.2023.108159
1001-8417/

energy between N-containing sites and pollutants is evaluated by density functional theory (DFT) calculations. Besides, the charge distribution and transfer number are also estimated in the process of SMX adsorption, which offers theoretical support for applications of biochar with N-containing adsorption sites at the molecular level. This study will provide a new perspective to better understand the adsorption mechanism of organic pollutants by biochar.

The cow dung was pyrolyzed at 500 °C with heating rate of 10 °C/min for 2 h in a N_2 atmosphere to obtain pristine biochar. Second, the potassium hydroxide and pristine biochar were mixed with mass ratio of 3:1. The mixture was then pyrolyzed at 500, 600, 700, 800 and 900 °C with heating rate of 10 °C/min for 2 h. The biochar was washed with deionized water and dried at 60 °C in a drying oven. The obtained samples were labeled as BC500, BC600, BC700, BC800 and BC900, respectively.

All materials and chemicals are given in Text S1 (Supporting information). Adsorption tests and analyses are shown in Text S2 (Supporting information). Characterization of BC are displayed in Text S3 (Supporting information). DFT calculations are described in Text S4 (Supporting information).

The adsorption data were fitted by *pseudo*-first-order and *pseudo*-second-order kinetic models (Eqs. 1 and 2).

$$\ln\,(q_e - q_t) = \ln\,(q_e) - k_1 t \tag{1}$$

$$\frac{t}{q_t} = \frac{1}{k_2 q_e^2} + \frac{t}{q_e} \tag{2}$$

where q_t is the adsorption amount of SMX (mg/g) at time t (min). q_e is the equilibrium adsorption capacity (mg/g); k_1 (min^{-1}) and k_2 (g mg^{-1} min^{-1}) represent the rate constants obtained by the *pseudo*-first-order and *pseudo*-second-order kinetic models.

The interactions of three N-related adsorption sites (graphite N, pyridinic N and pyrrolic N) were investigated by multiple non-linear fitting with 1stOpt 15 software based on Levenberg-Marquardt (LM) and universal global optimization (UGO) algorithms. The fitting model was defined as Eq. 3, which considered not only the role of a single site, but also the interactions between two or among three adsorption sites.

$$Y = AN_1N_2N_3 + BN_1N_2 + CN_2N_3 + DN_1N_3 + EN_1 + FN_2 + GN_3 \tag{3}$$

where N_1, N_2 and N_3 were the relative content of pyridinic N, pyrrolic N and graphite N. *A*, *B*, *C*, *D*, *E*, *F* and *G* referred to the coefficients. *Y* represented the adsorption rate.

The *pseudo*-second-order kinetic model presented a higher regression coefficient than the *pseudo*-first-order kinetic model (Table S1 in Supporting information), indicating the adsorption of SMX on cow dung-derived biochar was mainly dominated by chemisorption [16]. The adsorption rate Y (mg g^{-1} min^{-1}) of SMX can be calculated *via* Eq. 4 based on the *pseudo*-second-order kinetic model [17].

$$Y = k_2 q_e^2 \tag{4}$$

where q_e (mg/g) is the equilibrium adsorption capacity.

Fig. 1 showed the adsorption rate of different biochars towards SMX. Fig. S2 and Text S5 (Supporting information) displayed the adsorption rate of SMX by cow dung derived biochar. The adsorption rate of BC500 was only 3.3 mg g^{-1} min^{-1} due to low SSA of biochar (100.1 m^2/g, Table S2 in Supporting information) prepared at low temperature [18]. Not enough adsorption sits could be provided for SMX adsorption. In addition, the adsorption rate elevated from 3.3 mg g^{-1} min^{-1} to 126.9 mg g^{-1} min^{-1} dramatically with the temperature increasing from 500 °C to 700 °C. Higher temperature promoted the gasification of metal complexes on biochar surface, thereby facilitating the formation of pores [19]. As shown

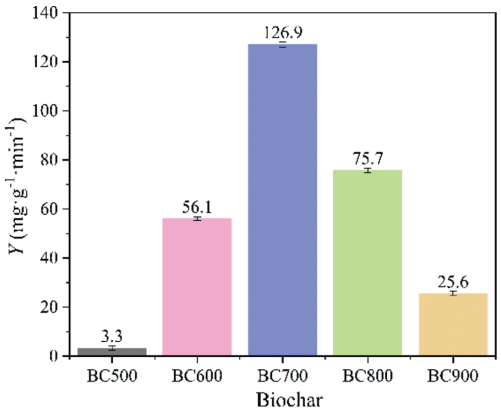

Fig. 1. Adsorption rate constants of different biochars ($[SMX]_0 =$ 15 mg/L, [Biochar] = 0.8 g/L, pH 5.14, T = 25 °C).

in Table S2, the total pore volume of biochar increased from 0.30 cm^3/g to 0.78 cm^3/g with temperature elevating from 500 °C to 700 °C. High temperature promoted the escape of volatile substances from biochar [20], so it was conducive to the formation of pore with the increase of temperature. Abundant pores with optimized pore structure might provide more adsorption sites for SMX removal under higher temperature. However, the adsorption rate of BC800 was only 75.7 mg g^{-1} min^{-1}, much lower than that of BC700 (126.9 mg g^{-1} min^{-1}) (Fig. 1). The pores of BC800 might be blocked by tar (Fig. S1 in Supporting information), resulting in a smaller SSA (675.7 m^2/g). In addition, the adsorption rate of BC900 was further decreased to 25.6 mg g^{-1} min^{-1}. The broken crosslinks and collapsed pores in the carbon matrix might lead to a significant reduction of the SSA of BC900 (223.9 m^2/g). Therefore, the optimal temperature for biochar preparation towards SMX adsorption was identified as 700 °C [21].

As shown in Table S2, the BC500 showed macroporous structure with pore size of 59.03 nm, which was much larger than the diameter of the SMX molecule (1.226 nm) [22]. Consequently, the larger pores mainly served as diffusion channels and reduced the interaction forces between the biochar and SMX [13]. Thus, BC500 had a relatively poor adsorption effect. As the temperature increased from 500 °C to 700 °C, the pore size dropped sharply from 59.03 nm to 16.49 nm. The reduction of pore size improved the retention capacity of biochar for SMX and increased the residence time of SMX in the pores, thus promoting the adsorption of SMX. Studies showed that carbonaceous materials with a pore size of 16.8 nm had superior adsorption capacity for organic matter [23]. The total pore volume of biochar decreased from 0.78 cm^3/g to 0.35 cm^3/g with temperature increasing from 700 °C to 900 °C. High temperature could destroy the pore structure and cause pore collapse, resulting in a downward trend in total pore volume. Therefore, the retention capacity of biochar to SMX would be further reduced with the expansion of pore size, which was not conducive to the adsorption of SMX.

The high-resolution N1s spectrum of biochar was deconvoluted into three peaks at 398.5, 399.6 and 400.7 eV, corresponding to the pyridinic N, pyrrolic N and graphitic N, respectively [24,25]. In addition, the total N content and the relative contents of N related-active sites in biochar were displayed in Fig. 2 and Table S3 (Supporting information). The total N content experienced a huge decrease from 12.0% to 5.9% with the pyrolysis temperature rising from 500 °C to 700 °C. Unstable N-containing substances and groups were decomposed continuously under higher pyrolysis temperature [26]. However, the generated tar would block the holes, limiting the consumption of N-containing substances when the temperature reached 800 °C [21]. Besides, the graphitic N

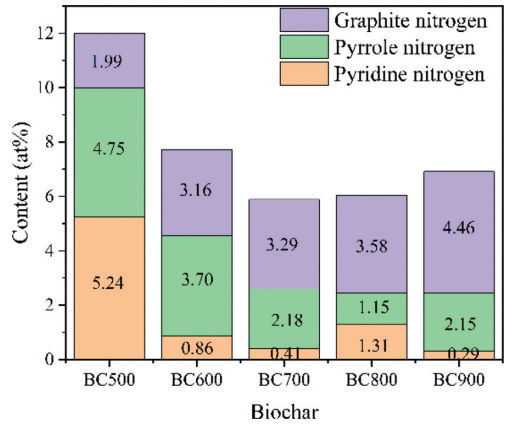

Fig. 2. Relative contents of N-related adsorption sites on cow dung-derived biochar surface.

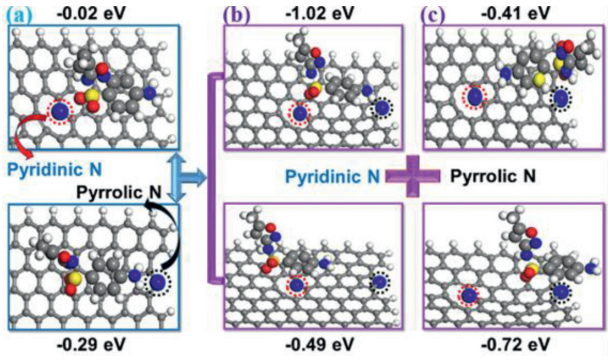

Fig. 3. The equilibrium configurations and adsorption energy of SMX on (a) pyridinic N, (b) pyrrolic N and (c) pyrrolic N-coupled pyridinic N sites. Red and black circles refer to pyridinic N and pyrrolic N, respectively.

content rose from 2.0% to 4.6% with the pyrolysis temperature increasing from 500 °C to 900 °C. Conversely, the proportion of pyrrolic N declined from 4.8% (BC500) to 1.2% (BC800). The structure of graphitic N was more stable than pyrrolic N. The C atoms in biochar were more easily replaced by N atoms to form graphitic N at higher pyrolysis temperature [27,28]. Furthermore, the content of pyridinic N in BC500 was as high as 5.2%, but stable around 1% at temperature higher than 500 °C. The pyrrolic N content decreased from 4.75 at% at 500 °C to 1.15 at% at 800 °C, attributing to the conversion of pyrrolic N to graphitic N [29]. In addition, the content of pyrrolic N increased from 1.15 at% to 2.15 at% when the temperature elevated from 800 °C to 900 °C, which was not conducive to the SMX adsorption by biochar. Thus, the pyrolysis temperature over 500 °C might have a minor influence on the content of pyridinic N.

The relationships between N-related adsorption sites and Y (mg g^{-1} min^{-1}) were analyzed *via* multivariate non-linear regression. The roles of N-related adsorption sites for SMX removal were displayed in Eq. 5.

$$Y = -17.02N_1N_2N_3 + 2.52N_1N_2 - 56.40N_2N_3 - 32.12N_1N_3 + 122.31N_1 + 193.62N_2 + 45.69N_3 \quad (5)$$

The full XPS and XRD spectra were provided to prove that there were no other potential metal adsorption sites in the carbon material (Fig. S3 and Text S6 in Supporting information). In addition, FTIR spectra demonstrated that the adsorption contributions of −OH, C−O−C and C=O groups on biochar surface to SMX removal could be eliminated (Fig. S4 and Text S7 in Supporting information).

Clearly, the factors of N_1, N_2 and N_3 in Eq. 5 were positive, indicating the significant role of single pyridinic N, pyrrolic N or graphitic N site in the process of SMX adsorption. In addition, the value of the coefficient indicated the contribution of the corresponding adsorption site. According to the individual adsorption sites, pyrrolic N had the largest contribution value, which was 1.58 and 4.24 times than pyridine N and graphite N. According to the literature, pyridinic N could combine with π electrons in aromatic ring of the organic pollutants to improve the π-π dispersion interactions [14]. In addition, the role of pyrrolic N was similar to that of −OH group, which could form hydrogen bonds with pollutants [30]. Furthermore, graphitic N could decline the π-electron density of biochar, strengthening the π-π electron donor-acceptor interactions between biochar and SMX [14].

The negative factors of N_2N_3 and N_1N_3 showed that the existence of graphitic N might compete with pyridinic N or pyrrolic N for the SMX adsorption. The absolute value of N_1N_3 was larger, indicating that graphite N and pyrrole N had a stronger antagonism. Similarly, negative factors of $N_1N_2N_3$ were also presented in Eq. 5. Obviously, no synergistic effect occurred among the three N-related sites. Noticeably, the positive factor of N_1N_2 (Eq. 5) indicated that the synergistic effect between pyridinic N and pyrrolic N could facilitate SMX adsorption.

The equilibrium configurations and adsorption energy of SMX on pyridinic N, pyrrolic N, pyridinic N-coupled pyrrolic N sites on biochar surface were shown in Fig. 3. To further explain the synergistic effect of pyridinic N and pyrrolic N on SMX adsorption, four adsorption equilibrium configurations were constructed with coexisting pyridinic N and pyrrolic N according to various contact modes between adsorption sites and SMX. As control, adsorption equilibrium configurations on single pyridinic N or pyrrolic N site were also established. The first-principles calculation was applied to calculate the adsorption energies of SMX on pyridinic N, pyrrolic N, and pyrrolic N-coupled pyridinic N sites. Adsorption energy indicated the stability of pollutant molecules on biochar surface [31]. Negative adsorption energy values represented the significant chemical interactions between organic matter and biochars [32]. Positive values indicated that external factors were required for the interaction of pollutants with biochars, implying the adsorption reaction was not prone to occur [33]. Obviously, the adsorption energy of SMX on pyrrolic N (−0.29 eV) was much higher than that on pyridinic N (−0.02 eV), revealing the stronger adsorption capacity of pyrrolic N site than that of pyridinic N towards SMX (Figs. 3a and b). The pyrrolic N might interact with organic contaminants by hydrogen bonding, playing a major role in SMX adsorption [14]. In addition, Fig. 3c depicted four optimized equilibrium configurations of SMX at the pyrrolic N-coupled pyridinic N adsorption site. The adsorption energies of SMX in the four coupling structures were calculated as −1.02, −0.41, −0.49 and −0.72 eV, which were 0.71, 0.10, 0.18, 0.42 eV higher than the sum of adsorption energies (−0.31 eV) on single pyrrolic N and pyridinic N sites, respectively. Clearly, the combination of pyridinic N and pyrrolic N could facilitate the adsorption of SMX.

To elucidate the interfacial mechanism during the adsorption of SMX by biochar at electronic level, the charge density distribution was collected and analyzed. Fig. 4. displayed the differential charge density distribution for the optimized adsorption configuration of pyrrolic N, pyridinic N and pyrrolic N-coupled pyridinic N sites. The blue and yellow parts represent the loss and gain of electrons, respectively. In addition, the overlapping electron indicated the affinity between biochar and SMX. Generally, a higher degree of overlap meant a stronger affinity [34]. Obviously, the electron cloud overlapped between biochar and SMX in all models. In addition, the electron sharing range of pyridinic N was lower than that of pyrrolic N due to the strong π-electron conjugation of the highest occupied molecular orbital (HOMO) of pyrrolic N. The HOMO

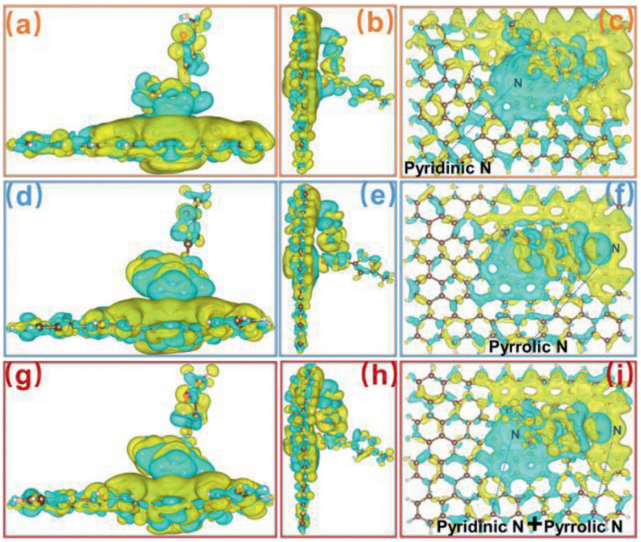

Fig. 4. The charge density difference of SMX adsorbed on (a-c) pyridinic N, (d-f) pyrrolic N and (g-i) pyrrolic N-coupled pyridinic N sites.

of pyrrolic ring was a π-orbital, while that of pyridinic ring was a p-orbital [35]. In comparison, the range of shared electrons in the pyrrolic N-coupled pyridinic N model was the widest. The coexistence of pyridinic N and pyrrolic N increased the π electron density of biochar. In consequence, the pyrrolic N-coupled pyridinic N adsorption sites had stronger interactions with SMX pollutants.

The Mulliken charge alteration of related atoms on biochar surface before and after adsorption of SMX was displayed in Table S4 (Supporting information). Extensive charge transfer occurred between adsorption sites and SMX. For a single adsorption site, the electron density around pyrrolic N atom increased by 0.094 e while that around pyridinic N decreased by 0.459 e after SMX adsorption. In the coexistence of pyridinic N and pyrrolic N, the electron density around pyrrolic N atom increased by 0.186 e, which decreased by 0.649 e around pyridinic N. The number of electrons transferred under both two N sites was larger than that obtained under single N site. Undoubtedly, the coexistence of pyridinic N and pyrrolic N enhanced the charge transfer between the two N-adsorption sites and SMX. As we know, the greater the amount of charge transfer, the stronger the electrostatic force between SMX and adsorption sites [36]. Therefore, the pyrrolic N-coupled pyridinic N adsorption sites had stronger electrostatic attraction to SMX. In addition, as shown in Table S5 and Fig. S5 (Supporting information), O1 atom lost 3.819 e and 2.861 e in the presence of pyridinic N and pyrrolic N sites alone, but there was no charge transfer in the existence of pyrrolic N-coupled pyridinic N site. In addition, no charge transfer was occurred in the O atoms at other positions and S atom. As shown in Table S6 and Fig. S6 (Supporting information), the charge transferred amount in carbon atoms adjacent to the nitrogen sites was zero, implying no charge transfer.

The interaction among N-related adsorption sites on cow dung-derived biochar surface towards SMX adsorption was explored systematically. The synergy between pyridinic N and pyrrolic N sites was witnessed during SMX adsorption. Besides, the adsorption energy values were higher towards SMX in the coexistence of pyridinic N and pyrrolic N than the sum of adsorption energies obtained by single pyridinic N and pyrrolic N, further confirming the positive effects between pyridinic N and pyrrolic N. In addition, the coexistence of pyridinic N and pyrrolic N enhanced the charge transfer between adsorption sites and SMX considerably, which had stronger electrostatic attraction to SMX. The obtained results could help to re-understand the contribution of active sites on the adsorbent surface to contaminants removal. Future research needs to further concentrate on the interactions among other adsorption sites to design highly-active adsorbents for water treatment.

Declaration of competing interest

The authors declare that they have no known competing financial interests or personal relationships that could have appeared to influence the work reported in this paper.

Acknowledgments

The authors would like to express gratitude to the National Natural Science Foundation of China (No. 52100156), Natural Science Foundation of Tianjin (No. 21JCQNJC00400) and Shenzhen Science and Technology Program (Nos. GJHZ20200731095801005 and JCYJ20200109150210400) for offering financial support to this research.

Supplementary materials

Supplementary material associated with this article can be found, in the online version, at doi:10.1016/j.cclet.2023.108159.

References

[1] D. Guo, S. You, F. Li, Y. Liu, Chin. Chem. Lett. 33 (2022) 1–10.
[2] Q. Zhang, S. Bolisetty, Y. Cao, et al., Angew. Chem. Int. Ed. 58 (2019) 6012–6016.
[3] M.R. Razanajatovo, W. Gao, Y. Song, et al., Chin. Chem. Lett. 32 (2021) 2637–2647.
[4] M. Ma, P. Dillon, Y. Zheng, Environ. Sci. Technol. 53 (2019) 10620–10628.
[5] J. Yan, J. Peng, L. Lai, et al., Environ. Sci. Technol. 52 (2018) 14302–14310.
[6] Y. Ren, W. Zheng, X. Duan, N. Goswami, Y. Liu, Environ. Func. Mater. 1 (2022) 10–20.
[7] Y. Song, X. Song, Q. Sun, et al., Sci. Total Environ. 803 (2022) 150087.
[8] H. Chen, J. Sun, Y. Song, et al., J. Colloid Interface Sci. 609 (2022) 676–685.
[9] Z. Sun, X. Wang, S. Xia, J. Zhao, Chem. Eng. J. 446 (2022) 137068.
[10] H. Zhan, Y. Wang, X. Mi, et al., Chin. Chem. Lett. 31 (2020) 2843–2848.
[11] G. Nie, S. Qiu, X. Wang, et al., Chin. Chem. Lett. 32 (2021) 2342–2346.
[12] X. Cao, L. Ma, B. Gao, W. Harris, Environ. Sci. Technol. 43 (2009) 3285–3291.
[13] X.F. Tan, S.S. Zhu, R.P. Wang, et al., Chin. Chem. Lett. 32 (2021) 2939–2946.
[14] Y. Cheng, B. Wang, J. Shen, et al., J. Hazard. Mater. 432 (2022) 128757.
[15] L. Xu, C. Wu, C. Chai, et al., J. Hazard. Mater. 424 (2022) 127606.
[16] J. Liu, W. Zhang, M. Mei, et al., Sep. Purif. Technol. 295 (2022) 121359.
[17] Y. Yan, H. Han, Y. Dai, et al., ACS Appl. Nano Mater. 4 (2021) 11763–11769.
[18] M.J.B. Evans, E. Halliop, J.A.F. MacDonald, Carbon 37 (1999) 269–274.
[19] S. Ding, Y. Liu, Fuel 260 (2020) 116382.
[20] H. Wang, X. Wang, Y. Cui, Z. Xue, Y. Ba, Bioresour. Technol. 263 (2018) 444–449.
[21] K. Li, D. Zhang, X. Niu, et al., Sci. Total Environ. 826 (2022) 154133.
[22] M.C. Tonucci, L.V.A. Gurgel, S.F.d. Aquino, Ind. Crops Prod. 74 (2015) 111–121.
[23] D. Crespo, R.T. Yang, Ind. Eng. Chem. Res. 45 (2006) 5524–5530.
[24] C. Liu, L. Chen, D. Ding, T. Cai, Appl. Catal. B 254 (2019) 312–320.
[25] R. Li, X. Lu, B. Yan, et al., Chem. Eng. J. 440 (2022) 135897.
[26] W.D. Oh, G. Lisak, R.D. Webster, et al., Appl. Catal. B 233 (2018) 120–129.
[27] G. Wang, S. Chen, X. Quan, H. Yu, Y. Zhang, Carbon 115 (2017) 730–739.
[28] Z.H. Sheng, L. Shao, J.J. Chen, et al., ACS Nano 5 (2011) 4350–4358.
[29] S.H. Ho, Y.d. Chen, R. Li, et al., Water Res. 159 (2019) 77–86.
[30] P. Zhang, H. Sun, L. Yu, T. Sun, J. Hazard. Mater. 244 (2013) 217–224 -245.
[31] W. Boumya, M. Khnifira, M. Abdennouri, et al., J. Mol. Struct. 1270 (2022) 133924.
[32] M. Du, Y. Zhang, Z. Wang, et al., Sep. Purif. Technol. 298 (2022) 121585.
[33] Q. Shi, L. Yan, T. Chan, C. Jing, ACS Appl. Mater. Interfaces 7 (2015) 26735–26741.
[34] Q. Chen, J. Zheng, L. Zheng, Z. Dang, L. Zhang, Chem. Eng. J. 350 (2018) 1000–1009.
[35] Q. Chen, J. Zheng, J. Xu, Z. Dang, L. Zhang, Chem. Eng. J. 356 (2019) 341–349.
[36] X. Sun, W. Liu, Z. Yang, et al., J. Mol. Liq. 334 (2021) 116145.